Responsive Polymers End-Tethered in Solid-State Nanochannels: When Nanoconfinement Really Matters

Mario Tagliazucchi,[†] Omar Azzaroni,[‡] and Igal Szleifer*,[§]

INQUIMAE, CONICET, Departamento de Química Inorgánica, Analítica y Química Física, Facultad de Ciencias Exactas y Naturales, Universidad de Buenos Aires, C1428EHA, Argentina, Instituto de Investigaciones Fisicoquímicas Teóricas y Aplicadas (INIFTA), CONICET, Departamento de Química, Facultad de Ciencias Exactas, Universidad Nacional de La Plata, CC 16 Suc.4 (1900) La Plata, Argentina, and Department of Biomedical Engineering and Chemistry of Life Processes Institute, Northwestern University, Evanston, Illinois 60208

Received May 14, 2010; E-mail: igalsz@northwestern.edu

Abstract: Solid state nanochannels modified with supramolecular architectures are a new and interesting class of stimuli-responsive nanofluidic element. Their fundamental understanding requires describing the behavior of soft-materials in confined geometries and its responses to changes in solution conditions. Here, a nanochannel modified with a polyelectrolyte brush is studied with a molecular theory that incorporates the conformational behavior of the polymers, electrostatic, van der Waals, and repulsive interactions coupled with the ability of the polymer segments to regulate their charge through acid−base equilibrium. The theory predicts pH-dependent ionic conductivity in excellent agreement with experimental observations. The polymer chains undergo large conformational changes triggered by variations in the outer solution environment and the conductivity of the device is shown to be controlled by the charge state of the polymer. The degree of polymer charge is largely affected by charge regulation and nanoconfinement effects. The molecular calculations show that the apparent pK_a inside the pore departs from that in solution when increasing the curvature of the nanochannel.

1. Introduction

Nanoscale fluidic channels are attracting widespread interest as a fundamental and technological challenge to chemists, physicists, and engineers.[1−4] Part of the appeal of nanochannels is their ability to control and manipulate the transport of ionic species flowing through them. These nanofluidic elements are promising building blocks for the construction of ionic circuits capable of sensing, switching, regulating, amplifying, or separating chemical species in aqueous solutions.[5−10] Nanofluidic channels with dimensions comparable to the range of the electrostatic interactions in solution display unique transport properties due to surface charge effects such as concentration enhancement and depletion and surface-charge-governed transport.[11−16] In those cases, interfacial effects rule the transport

properties of the device, in which the ions of the same charge as that of the walls are expelled from the nanochannel and the electrical current through it is primarily carried by the ions of opposite charge; that is, the nanoconfined environment becomes a "unipolar solution" of counterions.[17] One of the interesting questions which arose in recent years is whether it is possible to develop new nanochannel architectures which simulate natural supramolecular systems in that their functioning is determined by stimulus-triggered organization.

The synthesis of polymers inside the nanochannels emerged as a new frontier in the development of nanochannels with "smart" transport properties, provided that they can respond to external stimuli and modulate the surface charges. Such confined macromolecular assemblies would result in molecular and ionic gates through which species can be transported at will under the influence of externally tunable parameters.[18] Because of the structural and functional richness of macromolecular building blocks, the modification of the nanochannel walls with polymer brushes has proven very efficient in rendering stimuli-responsive

[†] Universidad de Buenos Aires.
[‡] Universidad Nacional de La Plata.
[§] Northwestern University.
(1) Daiguji, H.; Yang, P.; Szeri, A. J.; Majumdar, A. *Nano Lett.* **2004**, *4* (12), 2315–2321.
(2) Martin, C. R.; Siwy, Z. S. *Science* **2007**, *317* (5836), 331–332.
(3) van der Heyden, F. H. J.; Bonthuis, D. J.; Stein, D.; Meyer, C.; Dekker, C. *Nano Lett.* **2007**, *7* (4), 1022–1025.
(4) Schoch, R. B.; Han, J.; Renaud, P. *Rev. Mod. Phys.* **2008**, *80* (3), 839–883.
(5) Sparreboom, W.; Van Den Berg, A.; Eijkel, J. C. T. *Nat. Nanotechnol.* **2009**, *4* (11), 713–720.
(6) Dekker, C. *Nat. Nanotechnol.* **2007**, *2* (4), 209–215.
(7) Hou, X.; Jiang, L. *ACS Nano* **2009**, *3*, 3339–3342.
(8) Howorka, S.; Siwy, Z. *Chem. Soc. Rev.* **2009**, *38* (8), 2360–2384.
(9) Siwy, Z. S. *Adv. Funct. Mater.* **2006**, *16* (6), 735–746.
(10) Daiguji, H. *Chem. Soc. Rev.* **2010**, *39*, 901–911.
(11) Höltzel, A.; Tallarek, U. *J. Sep. Sci.* **2007**, *30* (10), 1398–1419.

(12) Kalman, E. B.; Vlassiouk, I.; Siwy, Z. S. *Adv. Mater.* **2008**, *20* (2), 293–297.
(13) Plecis, A.; Schoch, R. B.; Renaud, P. *Nano Lett.* **2005**, *5* (6), 1147–1155.
(14) Stein, D.; Kruithof, M.; Dekker, C. *Phys. Rev. Lett.* **2004**, *93* (3), 035901–1.
(15) Vlassiouk, I.; Siwy, Z. S. *Nano Lett.* **2007**, *7* (3), 552–556.
(16) Wanunu, M.; Meller, A. *Nano Lett.* **2007**, *7* (6), 1580–1585.
(17) Karnik, R.; Fan, R.; Yue, M.; Li, D.; Yang, P.; Majumdar, A. *Nano Lett.* **2005**, *5* (5), 943–948.
(18) Calvo, A.; Yameen, B.; Williams, F. J.; Azzaroni, O.; Soler-Illia, G. J. A. A. *Chem. Commun.* **2009**, (18), 2553–2555.

properties to these nanofluidic elements.[19] The very possibility of providing new avenues to incorporate responsive chemical functionalities into confined geometries marks an important advance in the development of "smart" nanofluidic systems. For example, the integration of pH-responsive poly(4-vinyl pyridine) (P4VP) brushes into solid state nanochannels enabled the construction of a nanofluidic device whose transport properties can be accurately controlled by manipulating the proton concentration in the surrounding environment.[20] The ionic current switching characteristics displayed by these nanochannels resemble the typical behavior observed in many biological channels that fulfill key pH-dependent transport functions in living organisms; that is, the nanochannel can be switched from an "off" state to an "on" state in response to a pH drop.

Despite the promising prospects, too little is known about the physicochemical characteristics of the inner environment of brush-modified nanochannels. While the previous example illustrates their functional versatility, a comprehensive understanding of fundamental aspects of nanochannels modified with polymer brushes remains elusive. To some extent, this uncertainty stems from limitations in addressing with molecular detail the local properties of surface-tethered protonable polymers, polyacids or polybases, in the electrolyte solution confined within the channel. The Poisson–Boltzmann and Poisson–Nernst–Planck approximations have been successfully applied to describe the ion concentration and the transport properties of nanochannels,[21−24] although their use has been limited to simple systems in which a formal constant charge density is confined on the pore walls. Due to the high degree of complexity of the experimental systems it is not surprising that analytical theories can only treat idealized and simplified scenarios. A major challenge is therefore to develop theoretical tools to describe and predict the rich molecular organization and electrostatic properties of supramolecular assemblies confined in nanochannels. These tools will serve as a guide for designing the next generations of functional nanofluidic elements.

Herein, we apply a molecular theory to understand and predict the behavior of the polymer modified nanopores. The theory explicitly accounts for molecular details of all the species inside the nanochannel and incorporates the molecular interactions and chemical equilibrium necessary for the proper treatment of protonable polymers.[25] The macroscopic observable, i.e., nanochannel conductance, predicted from the molecular theory is in excellent quantitative agreement with recently reported experimental observations for the case of nanochannels modified with P4VP brushes.[20] We show that molecular confinement gives rise to new forms of polymer organization and affects the acid–base equilibria and counterion distribution, directly impacting the transport properties of nanochannels and nanopores.
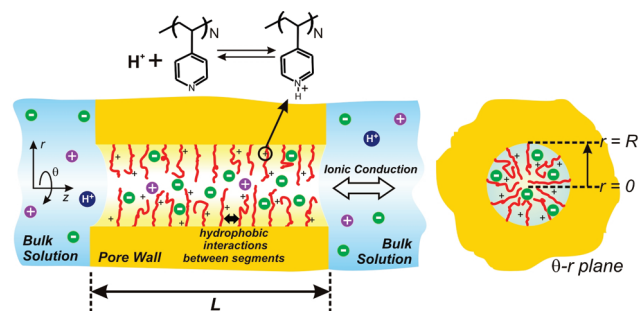

Figure 1. Schematic representation of the polyelectrolyte brush modified nanochannel. The cylindrical channel of radius R and length L ($L \gg R$) is modified with end-tethered chains of poly(4-vinyl pyridine). The 4-vinyl pyridine segments present effective vdW attractions (hydrophobic interactions) and can exist either in a positively charged protonated state or in a neutral deprotonated state. Switching between these two states is regulated by an acid−base equilibrium. The channel is connected to two macroscopic reservoirs containing aqueous solutions of K+, Cl−, protons, and hydroxyl ions in identical concentrations. Ion currents results upon applying an electric potential difference between the reservoirs.

2. Theoretical Basis

The system under study is schematized in Figure 1. It consists of a single cylindrical nanochannel modified with P4VP chains end-grafted to the inner surface. The pore is connected to two compartments containing solutions of controlled and identical composition (bulk solution). In order to model the structural and thermodynamic properties of this system, we use a previously reported molecular theory[25] extended to treat the proper geometry of the nanopore. The theory considers the size, charge, shape, and conformations of all of the molecular species in the system. Furthermore, this theoretical framework explicitly incorporates the delicate interplay between the acid−base equilibria, the physical interactions, the polymer conformational degrees of freedom, and the distribution of mobile species in the nanochannel. These are key elements that capture the physicochemical essence of functional responsive systems, like polymer brushes, facilitating a rigorous theoretical foundation ready to be implemented in advanced applications. For instance, in the past, its predictions have led to quantitative agreement with experimental results[26,27] and computer simulations[28] for a variety of planar polyelectrolyte layers under many different experimental conditions. In the present formulation of the theory, we consider only inhomogeneities in the radial direction (r) because the pore presents cylindrical symmetry and its length is much larger than its radius.

The theory considers N_P poly(4-vinyl pyridine) chains end-tethered to the inner surface of a cylindrical channel of radius R with an internal area $A(R)$. The grafting density is $\sigma = N_P/A(R)$. The pyridine group in each 4VP segment can be either protonated (pyH+) of deprotonated (py). In order to derive the theory we write down the free energy of the system as a functional of the probability distribution function of the polymer conformations, the densities of mobile species (water (w), K+, Cl−, H+, and OH−) and the interactions fields. These functions depend on r since we assume inhomogeneities only in the radial direction due to the geometry of the problem. The expression for the free energy per unit area is

(19) Yameen, B.; Ali, M.; Neumann, R.; Ensinger, W.; Knoll, W.; Azzaroni, O. *J. Am. Chem. Soc.* **2009**, *131* (6), 2070–2071.
(20) Yameen, B.; Ali, M.; Neumann, R.; Ensinger, W.; Knoll, W.; Azzaroni, O. *Nano Lett.* **2009**, *9* (7), 2788–2793.
(21) Vlassiouk, I.; Smimov, S.; Siwy, Z. *ACS Nano* **2008**, *2* (8), 1589–1602.
(22) Kosińska, I. D.; Goychuk, I.; Kostur, M.; Schmid, G.; Hänggi, P. *Phys. Rev. E* **2008**, *77* (3).
(23) Ramírez, P.; Mafé, S.; Alcaraz, A.; Cervera, J. *J. Phys. Chem. B* **2003**, *107* (47), 13178–13187.
(24) Vlassiouk, I.; Smirnov, S.; Siwy, Z. *Nano Lett.* **2008**, *8* (7), 1978–1985.
(25) Nap, R.; Gong, P.; Szleifer, I. *J. Polym. Sci., Part B* **2006**, *44*, 2638–2662.

(26) Gong, P.; Wu, T.; Genzer, J.; Szleifer, I. *Macromolecules* **2007**, *40* (24), 8765–8773.
(27) Tagliazucchi, M.; Calvo, E. J.; Szleifer, I. *J. Phys. Chem. C* **2008**, *112*, 458–471.
(28) Hehmeyer, O. J.; Arya, G.; Panagiotopoulos, A. Z.; Szleifer, I. *J. Chem. Phys.* **2007**, *126* (24).

$$\frac{\beta F}{A(R)} = \int_0^R \rho_w(r)[\ln(\rho_w(r)v_w) - 1]J(r)\,dr +$$

$$\int_0^R \rho_{Cl^-}(r)[\ln(\rho_{Cl^-}(r)v_w) - 1]J(r)\,dr +$$

$$\int_0^R \rho_{K^+}(r)[\ln(\rho_{K^+}(r)v_w) - 1]J(r)\,dr +$$

$$\int_0^R \rho_{H^+}(r)[\ln(\rho_{H^+}(r)v_w) - 1 + \mu^0_{H^+}]J(r)\,dr +$$

$$\int_0^R \rho_{OH^-}(r)[\ln(\rho_{OH^-}(r)v_w) - 1 + \mu^0_{OH^-}]J(r)\,dr +$$

$$\frac{N_P}{A(R)} \sum_\alpha P_P(\alpha)\ln P_P(\alpha) +$$

$$\int_0^R \int_0^R \frac{\beta\chi g(r,r')}{2}\langle\phi_P(r)\rangle\langle\phi_P(r')\rangle J(r)r'\,dr\,dr' +$$

$$\int_0^R \beta\pi(r)(\sum_i \rho_i(r)v_i + \langle\phi_P(r)\rangle)J(r)\,dr + \int_0^R \Big[\langle\rho_Q(r)\rangle\beta\psi(r) -$$

$$\frac{1}{2}\varepsilon\beta(\nabla_r\psi(r))^2\Big]J(r)\,dr + \int_0^R \langle n_P(r)\rangle[f_c(r)[\ln(f_c(r)) + \beta\mu^0_{pyH^+}] +$$

$$(1 - f_c(r))[\ln(1 - f_c(r)) + \beta\mu^0_{py}]]J(r)\,dr \quad (1)$$

where $\beta = 1/kT$ and the function $J(r) = A(r)/A(R) = r/R$ is the geometrical factor that takes into account the changes in the volume with r.[25] The first five terms in the free energy functional are the translational (mixing) entropies of the mobile species, with $\rho_i(r)$ being the number density of species i (i = w, K^+, Cl^-, H^+, and OH^-) at r and $\mu^0_{H^+}$ and $\mu^0_{OH^-}$ being the standard chemical potentials of protons and hydroxyl ions. The sixth term is the conformational entropy of P4VP chains. The seventh term models the effective vdW attractions between segments.[29] The constant χ gives the strength of the attraction forces and $\langle\phi_P(r)\rangle$ represents the volume fraction of the polymer at r. We refer the parameter χ to the critical value χ_c that is required to induce thermodynamic instability in a neutral planar polymer layer in the limit of vanishing surface coverage and it is close to the Θ conditions for the polymer backbone.[30,31] For P4VP we use $\chi_c/\chi = 0.6$ which corresponds to a hydrophobic backbone (i.e., poor solvent for the neutral polymer).

The eight term in eq 1 represents the intermolecular repulsions which are modeled as excluded volume interactions, with $\pi(r)$ being the repulsion field related to the local osmotic pressure which is determined from local packing constraints.[25] The ninth term in eq 1 is the electrostatic contribution to the free energy, where $\psi(r)$ is the local electrostatic potential, $\nabla_r\psi(r)$ is the gradient in the radial direction, ε is the dielectric constant and $\langle\rho_Q(r)\rangle$ is the average charge density at r, given by the sum of the charge densities of all of the mobile species and the polymer: $\langle\rho_Q(r)\rangle = \sum_i\rho_i(r)q_i + \langle n_P(r)\rangle f_c(r)q_P$, where $\langle n_P(r)\rangle$ is the average number density of polymer segments at r, q_i is the charge of species i in units of the elemental charge, and $f_c(r)$ is the fraction of protonated 4VP segments at r. The last integral in eq 1 is the chemical equilibrium term and it represents the mixing entropy between charged and uncharged segments, with $\mu^0_{pyH^+}$ and μ^0_{py} being their respective standard chemical potentials. These standard chemical potentials are related to the acid–base equilibrium constant of an isolated group in the bulk by $K^{bulk}_a = K_w/K^{bulk}_b = K_w/[C\exp(-\beta(\mu^0_{OH^-} + \mu^0_{pyH^+} - \mu^0_{py}))]$,[25,27] where C is a constant and $K_w = 10^{-14}$.

In order to find the equilibrium state of the system, eq 1 is minimized with respect to the unknown functions: $P_P(\alpha)$, $\rho_i(r)$, $\psi(r)$, and $f_c(r)$. The resulting set of coupled integro-differential equations is discretized in the r direction and solved numerically. Further details on analytical minimization and numerical implementation are given in the Supporting Information. The input for the theory includes a large representative set of 2×10^5 unbiased polymer

conformations, σ, χ_c/χ, pK^{bulk}_a, pH^{bulk}, C_{salt}, and R. The output of the theory provides the average r-dependent densities for all species, the local protonation fraction profile, the electrostatic potential, and the values of all thermodynamic quantities.

The averaged ion concentrations inside the pore can be calculated from the equation

$$\langle c_i\rangle = \frac{2}{R^2}\int_0^R c_i(r)r\,dr \quad (2)$$

where $c_i(r)$ is the molar concentration of the species i at r and zero bias potential predicted by the molecular theory and the mean dissociation fraction of PVP segments can be determined as

$$\langle f_c\rangle = \frac{\int_0^R f_c(r)\langle\phi_P(r)\rangle r\,dr}{\int_0^R \langle\phi_P(r)\rangle r\,dr} \quad (3)$$

In order to estimate the conductivity of the channel, the molecular theory is used in conjunction with the Nernst–Planck (NP) equation under the Goldman constant field (GCF) approximation.[23,24,32] Since we are dealing with long channels, the polarization contributions to the potential drop at channel/reservoir interfaces can be neglected.[24] Under these approximations, the ionic conductivity, G, results from the sum of the conductivities from all of the mobile ionic species (K^+, Cl^-, H^+, and OH^-), which are calculated using the diffusion coefficients for each ion and their average concentration inside the nanopore predicted by the molecular theory under zero applied potential. Assuming ion fluxes only in the z axis and equilibrium conditions in the pore entrances, the channel conductivity (G) is given by

$$G = I/V = \frac{2\pi}{L}\frac{F^2}{RT}\sum_{i=K^+,Cl^-,OH^-,H^+} q_i^2 D_i \int_0^R c_i(r)r\,dr \quad (4)$$

where D_i is the diffusion coefficient of species i.

The mean-field approximations underlying the NP has been predicted to be valid for channel radii larger than two Debye lengths (i.e., $R > 2$ nm in 0.1 M solution),[33–35] and the GCF approximation has been found to be in quantitative agreement with the full solution of NP–Navier–Stokes equations for pores longer than $\sim$100 nm.[24] The electroosmostic current neglected by reducing the NP–Navier–Stokes approach to the GCF approximation have been previously shown to have a very small effect on the total current through long nanochannels.[24] We will therefore limit our analysis to nanochannel dimensions within the ranges where this approximation is valid.

3. Results

3.1. Comparison with Experiments. The theory is aimed at predicting the experimental observations without the use of free adjustable parameters, provided that the molecular details of all of the species in the system are known. Figure 2 displays the experimental conductance values of a P4VP-modified single nanochannel as a function of the environmental pH, as recently reported by Yameen et al.[20] together with the theoretical predictions. For the experimental system the known parameters are the dimensions of the pore (radius, $R = 7.5$ nm, and length, $L = 12$ μm), the composition of the bulk solution and the

(29) Szleifer, I.; Carignano, M. A. *Adv. Chem. Phys.* **1996**, *96*, 165–260.
(30) Tagliazucchi, M.; Olvera de la Cruz, M.; Szleifer, I. *Proc. Natl. Acad. Sci.* **2010**, *107*, 5300–5305.
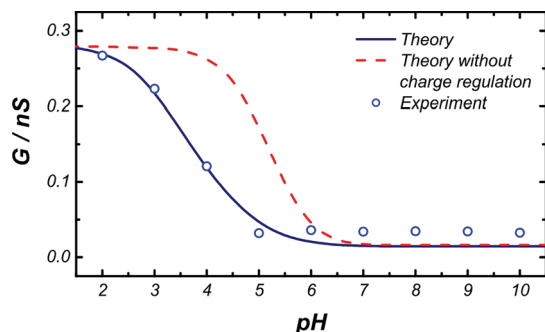(31) Gong, P.; Genzer, J.; Szleifer, I. *Phys. Rev. Lett.* **2007**, *98* (1), 018302–018304.

(32) Goldman, D. E. *J. Gen. Physiol.* **1943**, *27*, 37–60.
(33) Corry, B.; Kuyucak, S.; Chung, S. H. *Chem. Phys. Lett.* **2000**, *320* (1–2), 35–41.
(34) Corry, B.; Kuyucak, S.; Chung, S. H. *Biophys. J.* **2000**, *78* (5), 2364–2381.
(35) Moy, G.; Corry, B.; Kuyucak, S.; Chung, S. H. *Biophys. J.* **2000**, *78* (5), 2349–2363.

Figure 2. Comparison between experiment and theory. Experimental points were taken from ref 20 for the conductivity of a single pore of radius (R) 7.5 nm and length (L) 12 μm modified with a P4VP brush in 0.1 M KCl. Calculation parameters: σ (surface coverage) = 0.2 chains/nm^2, N (segments per chain) = 28, C_{salt} = 0.1 M, pK_a^{bulk} = 5.2. R = 7.5 nm, L = 12 μm, and χ_c/χ (strength of hydrophobic interactions) = 0.6. In the calculations without charge regulation the ionization fraction of the vinyl-pyridine segments was fixed to that of an isolated vinyl-pyridine group in the bulk, $f_{pyH+} = 1/(1 + K_a^{bulk}/[H^+]^{bulk})$.

acid−base constant for the pyridine-pyridinium equilibrium in solution (pK_a^{bulk} = 5.2[36]). Some additional parameters related to the molecular dimensions of the 4-vinyl pyridine (4VP) monomers can be estimated from molecular models or previous experimental measurements and are compiled in the Supporting Information. Since ca. 75−90% of the inner volume of the nanochannel is occupied by water the ions diffusion coefficients inside the pore were approximated by those measured in pure water.[36] The strength of segment−segment hydrophobic interactions was chosen to model the well-known hydrophobic properties of uncharged P4VP (preliminary calculations shown in Supporting Information showed that the conductivity curve is not very sensitive to the strength of the hydrophobic interactions). The degree of polymerization (N) and the surface coverage (σ) are unknown for this specific system, but can be estimated from experimental measurements on similar polyelectrolyte brushes. Figure 2 shows that an excellent agreement with the experimental measurements is obtained using σ = 0.2 nm^{-1} (reported for a planar brush prepared by a similar grafting technique[37]) and N = 28 (very close to the value N = 32 measured for polyelectrolyte brushes tethered inside mesoporous metal oxide films).[38]

3.2. Molecular Organization in the Nanopore. Figure 2 demonstrates that the molecular theory is able to quantitatively predict the experimental nanochannel conductance. Thus, the molecular theory can be used as an enabling tool for understanding the molecular basis of the ionic transport taking place in responsive nanochannels. In particular, the theory is very successful in predicting the exact pH of the inflection point, which is usually defined as the apparent pK_a (the bulk pH where the average protonation fraction is 0.5, pK_a^{app}) of the 4VP units inside the pore. The pK_a^{app} differs from the pK_a^{bulk} because the acid−base equilibrium is displaced toward the uncharged segments in order to minimize the local electrostatic repulsions in the system, a process known as charge regulation. This mechanism controls the net charge of the confined P4VP, which is different from that expected in free solution. The degree of

charge regulation depends on both the structure of the polymer layer as well as on the local density and distribution of free charges. Namely, the system optimizes its state by balancing the different free energy contributions to obtain a global equilibrium state. The reduction in the number of protonated pyridines carries with it a chemical free energy cost. However, this is more than compensated by the reduction in electrostatic repulsions associated with uncharging groups. Furthermore, there is also a gain in van der Waals attractions since reducing charge enables a larger local concentration of polymer segments.

The molecular theory explicitly considers the coupling that exists between all of the different chemical and physical interactions in the system (electrostatic, steric and hydrophobic forces, polymer conformational entropy, mixing entropy of mobile species and acid−base equilibrium) and therefore predicts their combined effect on charge regulation. Namely, the state of charge of the different groups is strongly coupled to the molecular organization, and the molecular organization is determined by the state of charge of the different groups. The optimization of the total free energy, including the spatial variation of all interactions and chemical states, i.e., charge state, is the only way to properly incorporate the coupling between charge regulation and molecular organization.

The question that arises though is how important is the competition between interactions and charge regulation or in other words, to what extent is charge regulation necessary to accurately predict ionic conductance. In Figure 2 we also show the calculated nanochannel conductance considering the degree of dissociation of the polymer segments in the channel to be equal to that of the monomers in the bulk solution (dashed line). As can be observed, this approximation fails to describe the experimental results. It is important to emphasize that the curve without charge regulation not only fails to predict the apparent pK_a but also has a shape that has important qualitative differences with the experimental measurements and the proper theoretical predictions. In particular, note that the conductance transition between the on/off states predicted by the theory without charge regulation occurs in a narrower pH range than that displayed by the experimental results. The broadening of the pH range observed in the real case arises from the fact that the degree of charge regulation and the structure of the polymer layer changes for each pH.

One of the strengths of the molecular theory is its ability to predict the molecular organization inside the pore, thus providing further insights on the mechanisms of ion conduction and pH responsiveness. Figure 3 shows the radial dependence of the polymer segment density for pH's 2 (open channel) and 10 (closed channel) for three different degrees of polymerization. For N = 28 the chains are extended at pH 2 in order to minimize electrostatic repulsions and collapse on the wall of the pore at pH 10 to maximize hydrophobic contacts between segments, as it was experimentally observed for P4VP grafted on planar[39] and spherical[40] surfaces. The system with N = 14 presents a similar behavior to that observed for N = 28, with the difference that at pH 2 the extended chains are not long enough to reach the center of the pore. On the other hand, the system with N = 55 presents a qualitatively different behavior: the polymers collapse to the center of the pore rather than on its walls. This is a nanoconfinement effect that occurs because the chain length

(36) *CRC Handbook of Chemical and Physics*, 72nd ed.; CRC Press: Boston, 1991.
(37) Jones, D. M.; Brown, A. A.; Huck, W. T. S. *Langmuir* **2002**, *18* (4), 1265–1269.
(38) Calvo, A.; Fuertes, M. C.; Yameen, B.; Williams, F. J.; Azzaroni, O.; Soler-Illia, G. J. A. A. *Langmuir* **2010**, *26*, 5559–5567.
(39) Ayres, N.; Boyes, S. G.; Brittain, W. J. *Langmuir* **2007**, *23* (1), 182–189.
(40) Li, D.; He, Q.; Yang, Y.; Möhwald, H.; Li, J. *Macromolecules* **2008**, *41* (19), 7254–7256.
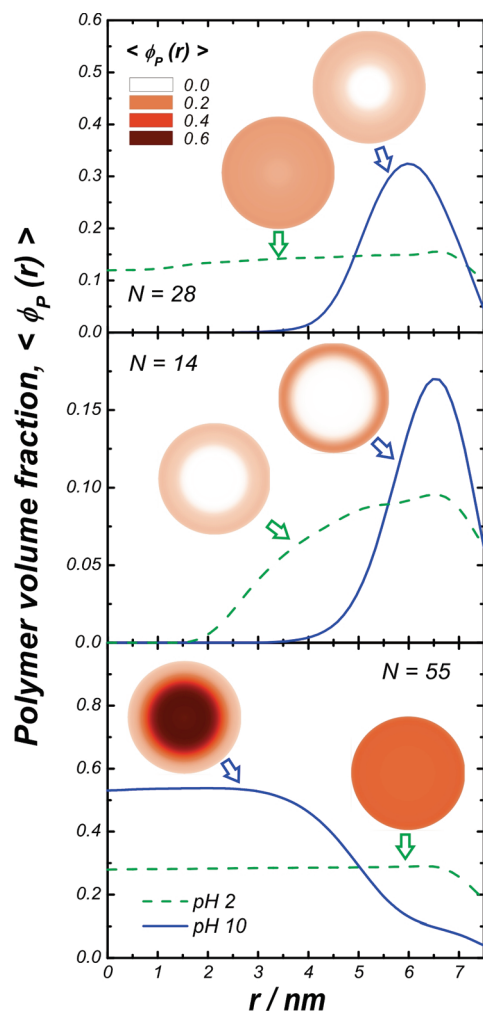
Figure 3. Polymer volume fraction as a function of the distance r from the pore center for different degrees of polymerization (N) and bulk pHs. Color maps show polymer distribution in $r-\theta$ the plane. Calculation parameters were $\sigma = 0.2$ chains/nm^2, $C_{salt} = 0.1$ M, p$K_a^{bulk} = 5.2$, $R = 7.5$ nm, and $\chi_c/\chi = 0.6$. The upper color scheme corresponds to that of the $r-\theta$ maps.

is long enough for the given pore radius to optimize hydrophobic collapse by maximizing the polymer–polymer contacts even at entropic cost of chain stretching. This mechanism is very similar to that of micellar formation in surfactant systems,[41] and the rules for the types of structure that will form depend on maximizing segment–segment hydrophobic contacts and minimizing water-segment contacts within the constraint that the polymer chains are end-grafted to the surface of the nanopore.[30] A proper understanding of the mechanisms of polymer collapse is important for the sterically controlled transport of larger solutes through nanochannels.[5] Namely, the understanding of the changes in charge within the nanopore as well as the structure of the polymer layer can be used for the selective transport of ionic moieties of different size by controlling the effective size of the pore when charged and uncharged. Furthermore, polymer swelling/collapse redistributes the solvent and mobile ions within the nanopore. Interestingly, our calculations show that at low pH there is an expulsion of solvent molecules (see Figure 3S in the Supporting Information). This effect arises because pyridine protonation requires coun-

(41) Gelbart, W. M.; Ben-Shaul, A. *J. Phys. Chem.* **1996**, *100* (31), 13169–13189.

terion uptake (see below) and since the inner volume of the nanopore is fixed water molecules are expelled to fulfill molecular packing.

We now consider in detail the experimental relevant case of $N = 28$ to determine what are the molecular factors and changes within the nanopore that determine the conductivity and its changes with pH. Changing pH from 10 to 2 results in a reorganization of the brush layer and in a different distribution of cations and anions within the channel. The conformational changes of the P4VP chains from a collapsed to an extended structure decrease the effective cross-section of the nanochannel, and consequently, this may be translated into a transmembrane ionic current decrease. The experimental results from Yameen et al. indicate that the transmembrane ionic current change is opposite to this argument.[20] This suggests that steric hindrance caused by polymer rearrangements is not the factor controlling the conductivity, which should be expected due to the relatively small size of the ions in the experimental settings. This conclusion is supported by the fact that the conductivity for the brush modified channel in the closed state, G (pH 10) = 0.015 nS is the same than that of an unmodified nanopore (i.e., a pore without grafted polymers and with uncharged walls) at the same pH. Moreover, the conductivity of the brush modified channel in the open state, G (pH 2) = 0.27 nS is much higher than that predicted for the unmodified channel at pH 2, G = 0.029 nS, indicating that conductivity is not blocked at high pH but enhanced in acidic solutions.

Figure 4a shows the radial dependence of K$^+$ and Cl$^-$ concentrations for pH's 2 and 10. At pH 10 (neutral polymer) the concentration of anions and cations are identical and close to the bulk value of 0.1 M, with the exception of a small depletion at $R \sim 6$ nm due to excluded volume interactions with the collapsed polymer brush. At pH 2 (positively charged brush), the Cl$^-$ concentration dramatically increases within the channel and reaches concentrations around 2 M, while the K$^+$ concentration drops to approximately 10^{-3} M. In other words, the pore displays anion permselectivity resembling a molecular scale scenario in which the inner environment of the channel represents a "unipolar" solution. Figure 4b compares the pH dependence of the nanochannel conductance, the average protonation fraction of the 4VP segments and the average concentration of K$^+$ and Cl$^-$. The theoretical predictions demonstrate that the factor controlling the transmembrane conductance is the large concentration of the majority charge carriers (Cl$^-$). The large concentration of anions within the pore is determined by the protonation fraction. Another interesting finding is that even though the pK_a^{app} of P4VP brushes is 3.7, Cl$^-$ and K$^+$ species equalize their concentrations within the nanochannel only at pH $\sim$8. The system requires an $\sim$4 pH unit increase above pK_a^{app} to restore the bulk electrolytic environment into the nanochannel. The reason is that the molecular interactions coupled with the acid–base equilibrium results in a broadening of the transition from protonated to unprotonated. This is manifested clearly in the experimental results, Figure 2, and the theoretical predictions where charge regulation is included. These results demonstrate the importance of the coupling between chemical equilibrium, physical interactions, and molecular organization in the determination of the properties of nanoconfined polymer layers.

An important parameter for nanopores that is related to ionic permselectivity is the ion selectivity ratio, S, defined here in analogy with ref 24 as $(I_{Cl^-} - I_<)/(I_{Cl^-} + I_<)$, where I_{Cl^-} is the current carried by the majority carrier (Cl$^-$) and $I_<$ is the sum
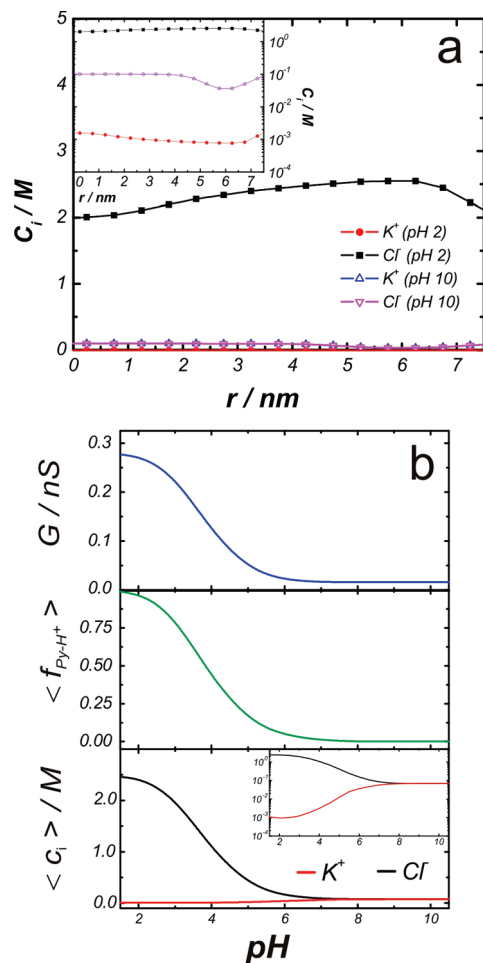
Figure 4. a. Concentration of salt ions, C_i (i = K^+ and Cl^-), as a function of the distance to the center of the pore. The inset shows the same results with the salt concentration in a logarithmic scale. The concentrations of K^+ and Cl^- at pH 10 are identical. b. pH dependence of channel conductivity, G, average fraction of protonated 4-vinyl-pyridine segments, $\langle f_{py\text{-}H+} \rangle$, and average concentration of salt ions, $\langle c_i \rangle$. The parameters used in the calculations correspond to the same case of Figure 3 with $N = 28$ (upper plot in Figure 3).

of the currents of the minority carriers (K^+, H^+, and OH^-). For pH 2 and the set of parameters used in Figure 4, theory predicts $S = 0.994$ ($S = 1$ corresponds to complete selectivity for Cl^-). As a comparison, a nanopore of the same radius bearing a fixed surface charge would require an unrealistically high surface charge larger than 3 |e| nm^{-2} in order to reach such selectivity and present a selectivity of only ~0.7 for a typical surface charge of 0.5 |e| nm^{-2}.[24] In other words, pore modification with grafted polyelectrolytes allows very high degrees of permselectivity that yield ion selectivities that cannot be achieved with other kinds of solid-state nanochannels.

In Figure 5 we present the polymer density, the electrostatic potential and the protonation fraction as functions of the radial distance for pH = pK_a^{app}. The decay of the electrostatic potential is determined by the distribution of the polymer chains rather than by the Debye length due to the charges in the polymers. Moreover, the nanopore dimensions are of the same order of magnitude as the polymer layer and therefore there is no bulk like region within the pore for the total decay of the electrostatic potential. The fraction of charged pyridines varies inversely to that of the polymer volume fraction. This is a direct manifestation of the interplay between chemical equilibrium and elec-
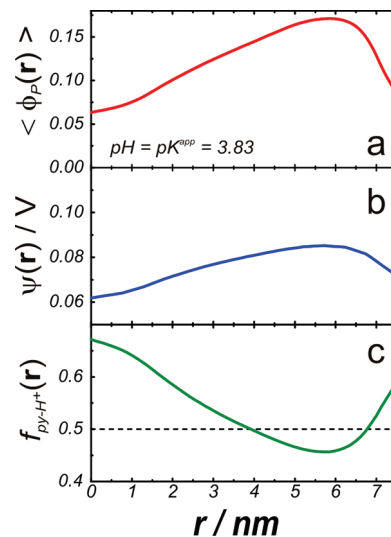

Figure 5. Radial profiles of polymer volume fraction (a), electrostatic potential (b), and fraction of protonated 4-vinyl-pyridine segments (c) for pH = pK_a^{app} = 3.83. The dashed line in the lower panel shows the average fraction of protonated vinyl-pyridine groups. σ = 0.2 chains/nm^2, C_{salt} = 0.1 M, pK_a^{bulk} = 5.2, R = 7.5 nm, χ_c/χ = 0.6, and N = 28.

trostatic interactions. As the polymer density increases, maintaining the fraction of charged groups results in large electrostatic repulsions and counterion confinement. The polymer segments have the option to unprotonate thus relaxing the electrostatic repulsion, increasing counterion release at the cost of chemical free energy. The results presented in Figure 5 show how the system optimizes under those specific conditions. This effect can be thought of as a local Le Chattelier principle.

3.3. Dependence of Nanopore Conductance on System Parameters. The molecular theory provides quantitative information about the molecular details of pH-responsive brushes confined in nanochannels and predicts the macroscopic experimental observations very well. It should also be used to establish and validate simple designing rules to create polymer modified nanofluidic devices with tailored responsive properties. As an example, the conductivity in the open state (pH 2) is an important design parameter that is expected to increase with the number of mobile ions per unit length. Assuming complete protonation of P4VP moieties, this quantity should be proportional to the number of polymer segments per unit length and thus to $N\sigma R$. Figure 6 shows that the predicted conductivity G at pH 2 increases linearly with $N\sigma R$ for several different combinations of R, N, σ, and salt concentration (C_{salt}), up to a value of the product around 50 nm^{-1}. The deviations to the universal behavior occur for large C_{salt}, N, and σ due to the nontrivial charge regulation and loss of permselectivity effects which are captured by the molecular theory but not by the simple argument discussed above.

Another important design parameter is the apparent pK_a, which provides the pH for the conductivity switching. Since this parameter is largely affected by charge regulation, the important question is how confinement of the polymer brush affects its ionization behavior and therefore its function. To answer this question we calculated the pK_a^{app} as a function of nanochannel radius (Figure 7a). A decrease in radius promotes a decrease in the apparent pK_a. Although it is well-known that
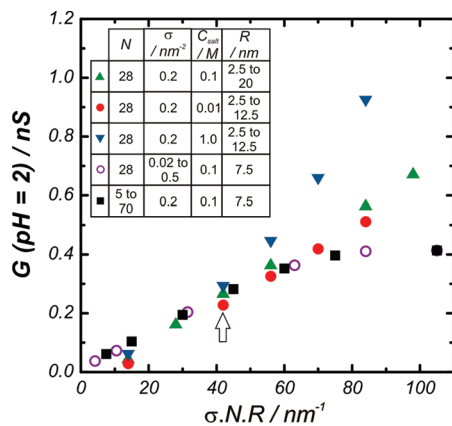
Figure 6. Pore conductivity predicted by the molecular theory in the open state (pH 2) as a function of σNR. The conductivity of the pore in Figure 2 is indicated with an arrow. The different conditions are indicated in the table inset.

pK_a^{app} is shifted with respect to the pK_a^{bulk} in planar brushes[31,42,43] and brushes in cylindrical geometry,[25] its dependence with the geometrical curvature has not been predicted for nanochannels. The large variation of pK_a^{app} with radius is primarily in the region where the radius is of the same order of magnitude as the thickness of the polymer brush. The origin of the effect is the following: due to the curvature of the channel the local concentration of 4VP segments (for a fixed grafting density) increases with the distance to the wall. A higher local segment concentration augments the electrostatic repulsions, inducing the deprotonation of pyridine groups and decreasing the pK_a^{app}. This effect can also be understood in terms of the local pH inside the pore ($pH^{channel}$). The presence of charged pyridinium groups exclude protons from the channel and thus $pH^{channel} > pH^{bulk}$ for the entire range of pH^{bulk} (see Figure 7b). The difference between $pH^{channel}$ and pH^{bulk} is higher for acidic solutions (higher fraction of protonated pyridines) and small channel radii (larger local concentration of pyridinium groups).

Figure 7c shows that the pK_a shift introduced by the curvature (defined as $\Delta pK_a^{app}(R) = pK_a^{app}(R) - pK_a^{app}(R \to \infty)$) scales with R^{-1} for large channel radii. This result is in good agreement with a simple model presented in the Supporting Information that considers the change in the local PVP segment concentration due to the curvature and predicts $\Delta pK_a(R) \sim -a/R$ (where a is a constant of the order of film thickness). The generalization of this argument to other geometries (i.e., polyelectrolyte brush modified nanoparticles[40]) is straightforward; that is, the apparent pK_a^{app} of a polybase tethered to a rod is expected to increase linearly with the inverse channel radius. In the small R regime (i.e., $R \ll a$) the charge regulation is a complex function of the molecular organization. In that case, a full account of the interactions and structure of the film is needed and the R^{-1} scaling law can be used only as an approximate guideline.

4. Conclusions

In summary, we presented a systematic theoretical study describing the molecular organization of nanofluidic elements modified with stimuli responsive polymeric building blocks. The excellent agreement between the experimentally observed
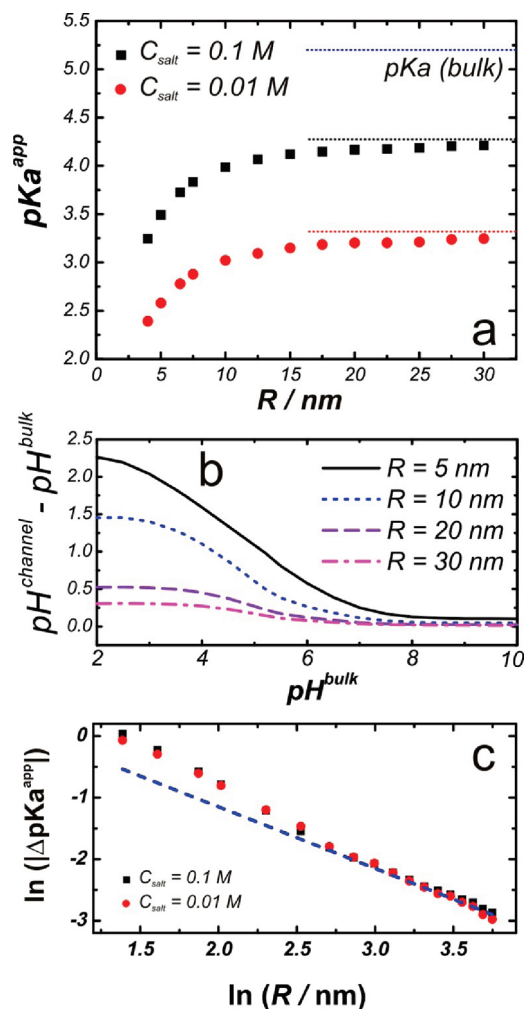
(42) Dong, R.; Lindau, M.; Ober, C. K. *Langmuir* **2009**, *25* (8), 4774–4779.
(43) Israëls, R.; Leermakers, F. A. M.; Fleer, G. J. *Macromolecules* **1994**, *27* (11), 3087–3093.

Figure 7. a. pK_a^{app} (defined as the pH where $\langle f_{py\text{-}H+} \rangle = 0.5$) as a function of pore diameter for two different salt concentrations. The blue dotted line shows the pK_a of vinyl-pyridine in the absence of interactions ($pK_a^{bulk} = 5.2$); black and red dotted lines show the apparent pK_a as calculated for the planar brushes. b. Difference between the pH inside the nanopore ($pH^{channel}$, defined as $-\log_{10}(\langle c_{H+} \rangle)$, with $\langle c_{H+} \rangle$ being the average proton molar concentration determined from eq 2) and pH^{bulk} as a function of the pH^{bulk} for $C_{salt} = 0.1$ M. c. Logarithm of $\Delta pK_a^{app}(R) = pK_a^{app}(R) - pK_a^{app}(R \to \infty)$ vs logarithm of pore radius for the calculations in panel a. The blue dashed line has a slope of -1. Calculation parameters: $N = 28$, $\sigma = 0.2$ chains/nm², and $\chi_c/\chi = 0.6$.

conductivity and the predictions of the molecular theory demonstrates the potential of this approach as a predictive tool to study the functional properties of ionic nanodevices and their variation with changes in the solution. The predictions of the molecular theory point out to the importance of properly treating the coupling between chemical equilibrium (charge regulation through protonation), molecular organization, and physical interactions within nanoconfined environments. Our results provide quantitative information regarding the chemical features and environmental conditions leading to the appearance of charge regulation effects, the formation of unipolar environments, and the generation of local ion and polymer depletion/enrichment regions. The theoretical description of the experimental conductance indicates that the ion transport characteristics are determined by electrostatic modulation originated from the presence of the polymer brush. In fact, brush-charge-mediated ionic transport was found to dominate in a wide range of proton

concentrations, whereas bulk-like behavior emerges only at pH's far above the pK_a^{app} of the P4VP brushes.

Our studies demonstrate the importance of nanoscale curvature effects on the dissociation equilibrium properties of responsive building blocks tethered on nanochannel walls. More importantly, we show that environmental stimuli, such as varying the pH, can trigger large conformational changes inside the pore. The very nature of these changes depends on the geometry of the imposed confinement, as was demonstrated here by the "collapse to the center" and "collapse to the walls" mechanisms. Taking advantage of these response mechanisms provides for novel pathways to create smart devices based on size-exclusion, in addition to charge, controlled transport.[44]

Nanofluidics represents an exciting discipline whose high standards are challenging to meet and, as a consequence, much of the inspiration to construct novel nanofluidic devices will heavily rely on the expansion and refinement of the physical picture that underlies their functional properties. On the other hand, modern experimental tools have resulted in an increased mastery in construction of functional macromolecules in nano-confined environments. In this context, theoretical frameworks are needed to understand and predict new emerging properties arising from polymers confined in nanometer length-scale regions. We believe that the theoretical framework presented in this work could become an integral part in the rational design of devices, as the theory provides fundamental understanding together with predictions of observable quantities.

Supporting Information Available: Detailed description of the numerical methods used to solve the molecular theory, figure showing the effect of the strength of hydrophobic interactions on the prediction of the pH-conductivity curve, the solvent volume fraction profiles for the case in Figure 3, and a simple model for the dependence of ΔpK_a with R in the large R limit. This material is available free of charge via the Internet at http://pubs.acs.org.

JA104152G

(44) Yavuz, M. S.; Cheng, Y.; Chen, J.; Cobley, C. M.; Zhang, Q.; Rycenga, M.; Xie, J.; Kim, C.; Song, K. H.; Schwartz, A. G.; Wang, L. V.; Xia, Y. *Nat. Mater.* **2009**, *8* (12), 935–939.